JACS
JOURNAL OF THE AMERICAN CHEMICAL SOCIETY
Article
pubs.acs.org/JACS

Biphenalenylidene: Isolation and Characterization of the Reactive Intermediate on the Decomposition Pathway of Phenalenyl Radical

Kazuyuki Uchida,[†] Soichi Ito,[‡] Masayoshi Nakano,*[,‡] Manabu Abe,*[,§] and Takashi Kubo*[,†]

[†]Department of Chemistry, Graduate School of Science, Osaka University, Toyonaka, Osaka 560-0043, Japan

[‡]Department of Materials Engineering and Science, Graduate School of Engineering Science, Osaka University, Toyonaka, Osaka 560-8531, Japan

[§]Department of Chemistry, Graduate School of Science, Hiroshima University, 1-3-1 Kagamiyama, Higashi-Hiroshima, Hiroshima 739-8526, Japan

Supporting Information

ABSTRACT: First isolation and characterization of biphenalenylidenes, which have long been unidentified reactive intermediates on the decomposition pathway of phenalenyl radical, were accomplished. Photoinduced electrocyclic ring-opening reaction of *anti*-dihydroperopyrene resulted in a successful conversion to *E*-biphenalenylidene, which enabled a detailed investigation of the electronic structure of *E*-biphenalenylidene by means of spectroscopic techniques. A stereoisomer, *Z*-biphenalenylidene, was also observed by suppressing a facile *E*−*Z* isomerization to *E*-biphenalenylidene in a rigid matrix. Furthermore, *Z*-biphenalenylidene demonstrated a thermal ring-closure in conrotatory process, which is not conforming to the Woodward−Hoffmann rule. These unusual reactivities of biphenalenylidene are ascribed to the ground states destabilized by its singlet biradical character, which was fully supported by theoretical calculations. The presence of *E*-biphenalenylidene on the decomposition pathway of phenalenyl was confirmed experimentally, leading to the full understanding of the decomposition mechanism of phenalenyl.

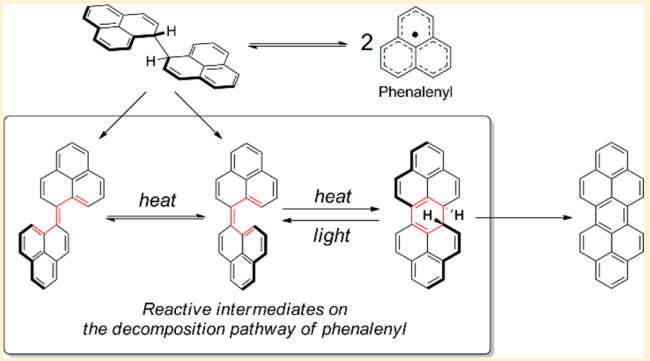

INTRODUCTION

Phenalenyl is an odd-alternant hydrocarbon radical stabilized thermodynamically by the delocalization of an unpaired electron over six α carbon atoms,[1] and has attracted much interest due to its fascinating solid state properties[2−4] and unique self-association behaviors.[5−8] First isolation of phenalenyl radicals in solid state was accomplished by introducing *tert*-butyl groups at three β carbon atoms.[9] The steric protection by substituted groups improved the kinetic stability, leading to a successful isolation and characterization in solution and solid state.[10,11] Various phenalenyl derivatives with steric and electronic perturbations have been synthesized and isolated.[7,8,12,13] Nevertheless, the parent phenalenyl (**1**) has not yet been isolated because of the kinetic instability resulting in a facile decomposition. Early attempts to synthesize **1** were reported in 1950s. Although preparation from several precursors gave blue or green products including **1**,[14−16] the isolation was unsuccessful due to the rapid conversion into a decomposed product. The decomposed product was doubtlessly assigned to peropyrene (**4**),[15,16] which would be generated by the dehydrogenation of $\mathbf{1}_2$ σ-dimer. The product analysis suggested that *E*- and *Z*-biphenalenylidene (*E*,*Z*-**2**) and dihydroperopyrene (**3**) should be the reactive intermediates on the decomposition pathway of **1** (Scheme 1), whereas experimental detection of these compounds has long been unsuccessful. In 2003, an experimental attempt was demonstrated by Agranat et al. to synthesize **2** directly.[17] Desulfurization followed by dimerization of phenalenethione afforded a green product that shows a broad absorption band at 647 nm in the electronic absorption spectrum. Unfortunately, the rapid decomposition into **4** prevented the detailed characterization and isolation of the colored species. To detect and characterize the intermediates, a moderate synthetic approach is required.

We here present the first isolation and characterization of *E*,*Z*-**2** in solution state. Successful preparation of *E*,*Z*-**2** was accomplished by a photoinduced electrocyclic ring-opening reaction of a *RR*/*SS* form of **3** (*anti*-**3**) synthesized efficiently from a phenalene derivative. Clean conversion of *anti*-**3** to *E*,*Z*-**2** enabled us to estimate the intriguing electronic structures, including the contribution of singlet biradical character, on the basis of spectroscopic techniques. Moreover, the unusual reactivity, which was ascribed to the singlet biradical characters of *E*,*Z*-**2**, was fully investigated experimentally and theoretically. Finally, the decomposition mechanism of **1** in the presence of an oxidizing reagent was unambiguously clarified by detecting *E*-**2** directly on the decomposition pathway.

Received: December 24, 2015

DOI: 10.1021/jacs.5b13033
J. Am. Chem. Soc. XXXX, XXX, XXX−XXX

Scheme 1. Proposed Mechanism of the Decomposition Pathway of 1[17]

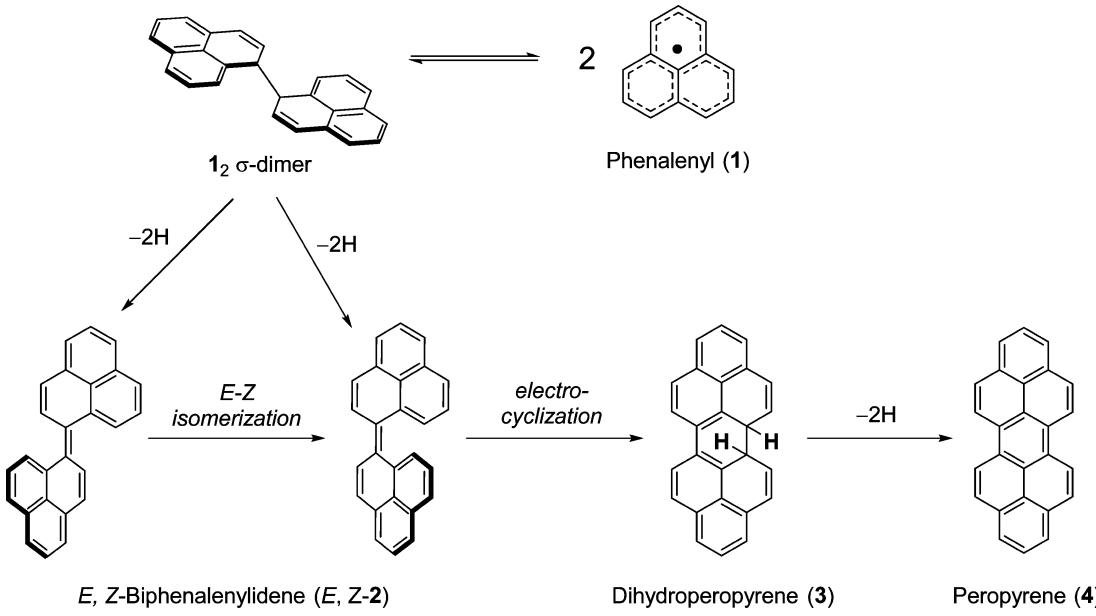

RESULTS

Synthesis of Dihydroperopyrene (3). Dehydrogenation of phenalene derivatives is an effective way to synthesize the corresponding phenalenyl radicals in mild conditions. The key precursor, biphenalene **11**, was obtained according to the synthetic scheme displayed in Scheme 2. Dibromobinaphthalene **6** prepared from binaphthalene **5** was converted into the unsaturated ester **7** by the Heck reaction. Hydrogenation of C−C double bonds and subsequent hydrolysis in basic condition gave the carboxylic acid **9**, and then Friedel−Crafts cyclization of the acyl chloride derived from **9** afforded biphenalanone **10** in remarkable yield. Reduction followed by dehydration gave biphenalene **11**. Treatment of **11** with an equimolar *p*-chloranil under nitrogen atmosphere gave a deep blue solution in the early stage of the reaction, and subsequent stirring in the dark resulted in a gradual color change from deep blue to greenish yellow. The product obtained by the dehydrogenation showed a well-resolved ^{1}H NMR spectrum as shown in Figure 1. A characteristic singlet peak that appeared at 4.4 ppm was assignable to benzyl protons on the phenalene scaffold, and the product was unambiguously characterized to **3** on the basis of 2D-NMR techniques as well as the computational prediction of NMR chemical shifts with a GIAO-B3LYP/6-31G** method (Figure S1 in Supporting Information).

Dihydroperopyrene (**3**) has two possible stereoisomers, a diastereomeric pair of **3** *RR*/*SS* form (*anti*-**3**) and **3** *RS* form (*syn*-**3**), originating from two asymmetric carbon atoms at the central six-membered ring. Molecular geometries of *anti*-**3** and *syn*-**3** estimated with a B3LYP/6-31G** method were displayed in Figure 2. *Anti*-**3** adopted an almost planar structure with C_2 symmetry; in contrast, *syn*-**3** demonstrated a highly distorted conformation with C_1 symmetry. The structural difference between the diastereomers is crucially reflected on the relative energy; that is, *syn*-**3** with the structural distortion is 11.8 kcal mol^{-1} (1 kcal mol^{-1} = 4.184 kJ mol^{-1}) less stable in energy than *anti*-**3**, which is almost identical to that estimated by Agranat et al. (12.1 kcal mol^{-1} at B3LYP/6-31G* level).[17] This computational result suggests that the experimentally obtained **3** should adopt the energetically favored *anti*-configuration. Single crystals of **3** were grown by slow evaporation of a chloroform/hexane solution under argon atmosphere to elucidate the molecular geometry by X-ray crystallographic analysis. Although the geometry obtained includes a structural ambiguity around the sp^3 carbon atoms due to the disordered alignment of **3** *RR* and *SS* isomers in crystalline state, the planar molecular backbone corroborates the *anti*-configuration of **3** (Figure S2 in Supporting Information). ^{1}H NMR spectrum may support this assignment. As shown in Figure 1, **3** gave a simple spectrum arising from a single diastereomer with magnetically equivalent two phenalenyl sites. The simplicity of ^{1}H NMR spectrum evokes two possibilities: (1) **3** obtained adopts the *anti*-configuration with C_2 symmetry, (2) **3** adopting the *syn*-configuration gives an averaged spectrum due to the dynamic equilibrium between stable C_1 conformations. To exclude the possibility of the dynamic equilibrium, variable temperature (VT) ^{1}H NMR was conducted within the temperature range from 298 to 183 K. **3** showed no signal splitting even at 183 K, inferring that **3** adopts the *anti*-configuration having an essential C_2 geometry. The result is consistent with the computational prediction that **3** adopts the energetically preferred *anti*-configuration. However, it should be noted that the possibility of the dynamic equilibrium was not strictly excluded. The activation barrier for the conformational change of *syn*-**3**, which was estimated with a broken-symmetry (BS) UB3LYP/6-31G** method, was extremely small (2.3 kcal mol^{-1}), and thus, an averaged spectrum might be observed even at 183 K.

Preparation and Characterization of *E*-Biphenalenylidene (*E*-2). With a focus on the electronic structure, *anti*-**3** can be regarded as a 1,3-cyclohexadiene analogue, which is a well-known scaffold that demonstrates the electrocyclic ring-opening reaction to afford a *cis*-1,3,5-hexatriene structure. As predicted by the Woodward−Hoffmann rule based on the orbital symmetry considerations, 1,3-cyclohexadiene scaffold undergoes a photochemically allowed ring-opening reaction in conrotatory mode; thus, *anti*-**3** would be converted into *Z*-**2** by the photoirradiation.

DOI: 10.1021/jacs.5b13033
J. Am. Chem. Soc. XXXX, XXX, XXX−XXX

Scheme 2. Synthetic Procedure for 3[a]

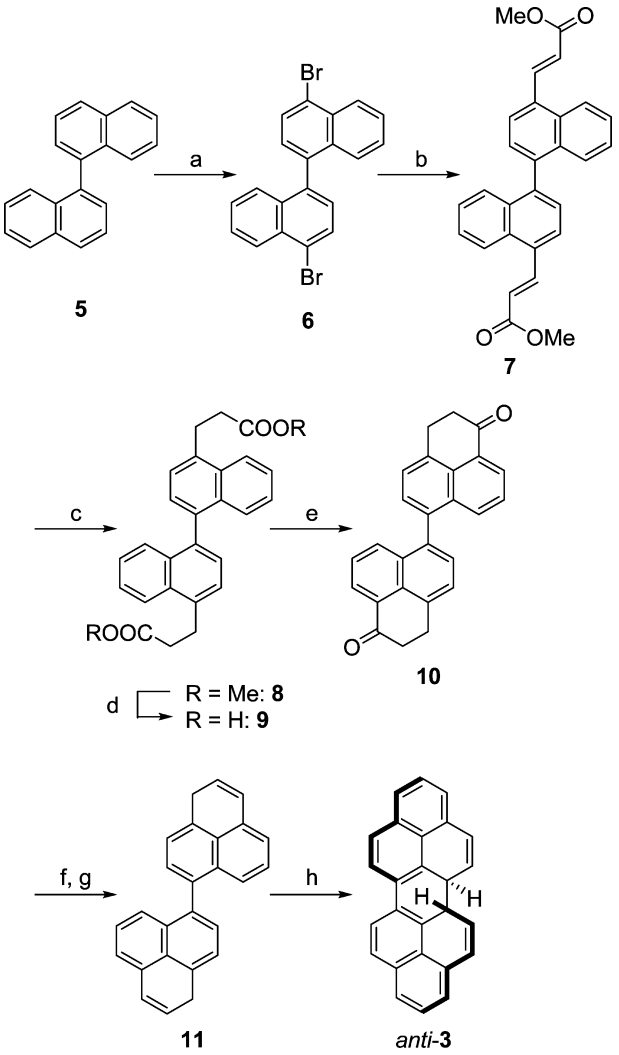

[a]Reagent and condition: (a) bromine, $CHCl_3$, 0 °C, 64% yield; (b) methyl acrylate, $Pd(OAc)_2$, PPh_3, K_2CO_3, $^nBu_4NBr$, DMF, 80 °C, 93% yield; (c) H_2 (1 atm), 10% Pd–C, DCM/AcOEt (1/9), RT, 88% yield; (d) 10% NaOH(aq), EtOH, 90 °C, 94% yield; (e) (i) $(COCl)_2$, 60 °C, (ii) $AlCl_3$, DCM, −78 to −30 °C, 88% yield; (f) $NaBH_4$, DCM/EtOH (1/1), RT; (g) *p*-TsOH·H_2O, toluene, 120 °C, 92% yield (2 steps); (h) *p*-chloranil, toluene, RT, 24% yield. *p*-Chloranil = 2,3,5,6-tetrachloro-1,4-benzoquinone.

Irradiation of UV light (365 nm) to *anti*-**3** in degassed dichloromethane-d_2 resulted in a dramatic change in ^{1}H NMR spectrum, accompanied by a noticeable color change from yellow to deep blue. ^{1}H NMR spectrum recorded after the irradiation was shown in Figure 3, together with the spectrum of *anti*-**3** measured before irradiation. Upon irradiation for 30 s, *anti*-**3** was converted quantitatively into a single product. The species was unambiguously characterized to the long-unidentified intermediate **2** by 2D-NMR spectroscopy as well as the computational calculation of the NMR chemical shifts conducted at GIAO-UB3LYP(BS)/6-31G** level (Figure S3 in Supporting Information). The stereochemistry of **2** observed in ^{1}H NMR spectrum was determined by a ROESY measurement conducted at 223 K (Figure S3b). **2** showed cross peaks between H_a and H_h in opposite sign with respect to diagonal peaks, which indicates that H_a and H_h are in close proximity to each other. Thus, **2** observed adopts the *E*-configuration. It is expected that an initial product of the photoinduced ring-opening reaction is *Z*-**2**, and therefore, a rapid isomerization from a metastable *Z*-**2** to energetically favorable *E*-**2** would take place.[17]

A progressive signal broadening was observed in ^{1}H NMR spectra of *E*-**2** upon raising temperature, and the signals almost disappeared at 253 K (shown in Figure 4). In general, the signal broadening is caused by a slow exchange due to molecular motions. Although *E*-**2** is expected to undergo *E*−*Z* isomerization to *Z*-**2** by the rotation about the central double bond upon increasing temperature, the disappearance of the signals cannot be accounted for by the molecular motion. On the other hand, the presence of paramagnetic species, such as metal impurities and radical species, also induces the signal broadening. We here focused on the singlet biradical ground states of *E*,*Z*-**2** predicted by Agranat et al. on the basis of theoretical calculations.[17] Twisted geometries of **2** arising from the overcrowding in *cove* region of *E*-**2** and *fjord* region of *Z*-**2** result in the decrease of spatial overlap between two unpaired electrons on phenalenyl sites, leading to the enhancement of the singlet biradical nature of *E*- and *Z*-**2**. The singlet biradical species having small energy gaps (ΔE_{S-T}) between the singlet ground state and the excited triplet state are known to show broad NMR spectra due to the existence of thermally excited triplet species.[18−22] Actually, ΔE_{S-T} values of *E*-**2** and *Z*-**2** were estimated by theoretical calculations to be 4887 K (9.7 kcal mol^{-1}) and 2084 K (4.1 kcal mol^{-1}), respectively, which are small enough to demonstrate the signal broadening in ^{1}H NMR spectra. Thus, the presence of thermally excited triplet species of *E*,*Z*-**2** resulted in the signal broadening in the ^{1}H NMR spectra, corroborating the singlet biradical ground states of *E*,*Z*-**2**.

The electrocyclic ring-opening reaction of *anti*-**3** was also monitored by the electronic absorption measurement. *anti*-**3** showed no characteristic absorption band in visible region, whereas *E*-**2** generated by photoirradiation showed an intense absorption band centered at 619 nm (Figure 5). This result is fairly consistent with the computational prediction by a time-dependent (TD) UB3LYP(BS)/6-31G** calculation that the HOMO−LUMO transition of *E*-**2** is located at 720 nm (f = 0.384). Notably, *Z*-**2** is expected to show its HOMO−LUMO transition at 859 nm (f = 0.106); however, the absorption band corresponding to *Z*-**2** was not observed in the electronic absorption spectrum because of the rapid isomerization to *E*-**2**.

Direct Observation of *Z*-Biphenalenylidene (*Z*-2). *Z*-**2**, which is the key intermediate on the photoinduced ring-opening process, was observed directly by suppressing the rotation about the central double bond. The electronic absorption spectrum was monitored in a glassy 2-methyltetrahydrofuran (MTHF) matrix at 98 K. Irradiation of UV light (355 nm) to *anti*-**3** in a rigid matrix of MTHF resulted in the appearance of a broad absorption band centered at 700 nm (Figure 6a), which is assignable to the HOMO−LUMO transition of *Z*-**2** on the basis of a TD-UB3LYP(BS)/6-31G** calculation (859 nm, f = 0.106). The absorption band remained unchanged in a MTHF matrix for a long time, indicating that *Z*-**2** is persistent in a condition that the rotation about the central double bond is suppressed kinetically. A substantial change was observed in the electronic absorption spectrum with increasing the temperature to 120 K (Figure 6b), where a viscosity of a MTHF matrix dramatically changes from 10^7 to 10^3 P.[23] The differential spectra were dominated by the bleaching of an absorption band at 700 nm and by growing with maximum at

DOI: 10.1021/jacs.5b13033
J. Am. Chem. Soc. XXXX, XXX, XXX−XXX

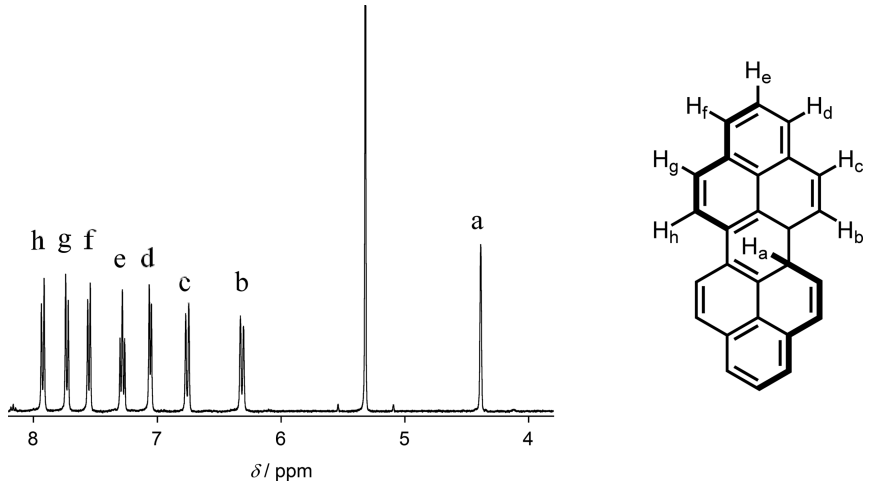

Figure 1. ^{1}H NMR spectrum of **3** measured in dichloromethane-d_2.

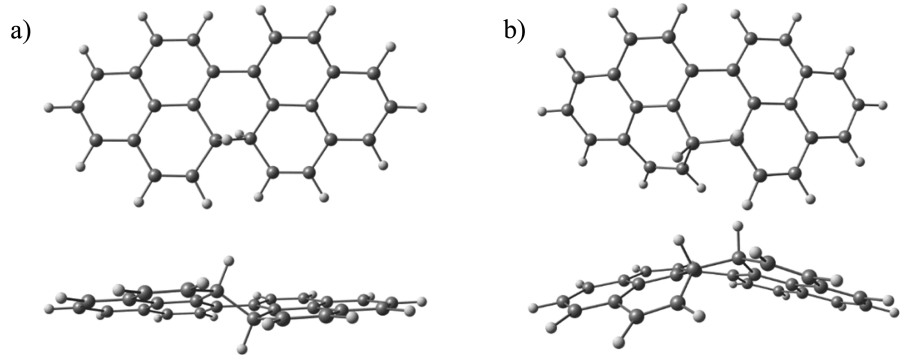

Figure 2. Optimized geometries of (a) *anti*-**3** and (b) *syn*-**3** determined by a UB3LYP(BS)/6-31G** method.

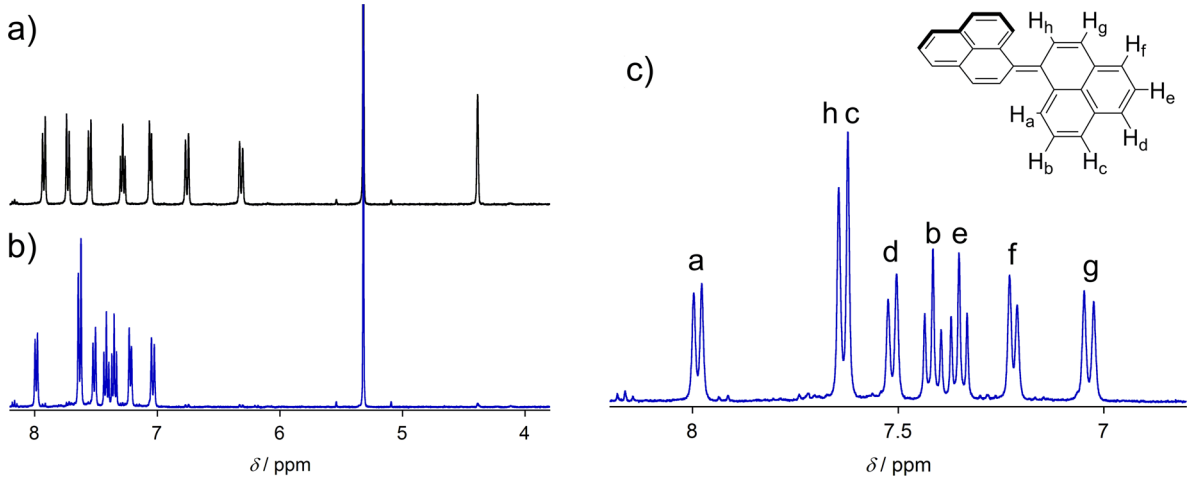

Figure 3. ^{1}H NMR spectra recorded in degassed dichloromethane-d_2 at 183 K (a) before irradiation and (b) after irradiation of UV light (365 nm) for 30 s. (c) Magnified view of aromatic region.

630 nm, suggesting the relaxation of a MTHF matrix leads to the thermal isomerization of *Z*-**2** to *E*-**2** by the rotation about the central double bond. The kinetics of the rapid thermal isomerization was investigated by the transient absorption spectrum within the temperature range from 183 to 203 K. The absorption of *Z*-**2** monitored at 705 nm decayed with a simple first-order kinetics, and the absorption of *E*-**2** grew with the same rate constant as the decay rate constant of *Z*-**2** (Figure 6c), which indicates that *Z*-**2** is directly converted into *E*-**2** through thermal isomerization. From the temperature dependence of the decay rate constant, the activation barrier of the thermal isomerization from *Z*-**2** to *E*-**2** was determined to be 4.3 ± 0.3 kcal mol^{-1} (log*A* = 12) by using Arrhenius plot (shown in Figure 6d).

Thermal Ring-Closure Reaction of Biphenalenylidene. According to the Woodward−Hoffmann rule, interconversion between *anti*-**3** having a 1,3-cyclohexadiene structure and *Z*-**2** having a *cis*-1,3,5-hexatriene structure is expected to take place

DOI: 10.1021/jacs.5b13033
J. Am. Chem. Soc. XXXX, XXX, XXX−XXX

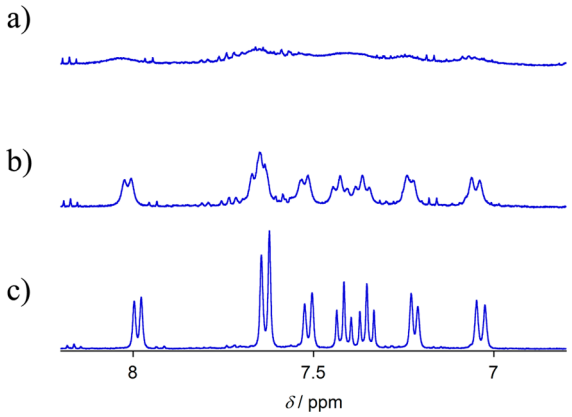

Figure 4. VT ^{1}H NMR spectra of *E*-**2** measured in dichloromethane-d_2 at (a) 253 K, (b) 223 K, and (c) 183 K.

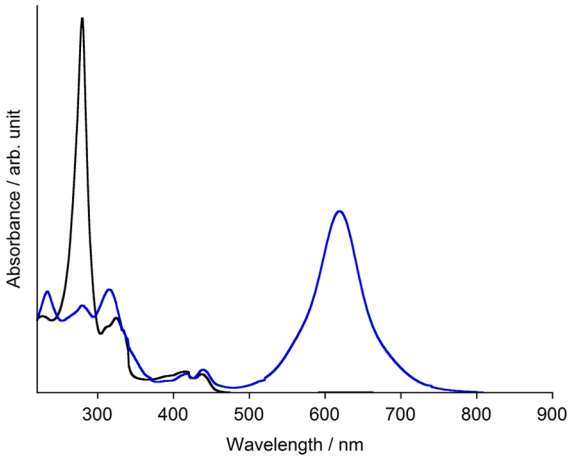

Figure 5. Electronic absorption spectra of *E*-**2** (blue) and *anti*-**3** (black) measured in dichloromethane (1×10^{-5} M). *E*-**2** was generated by UV irradiation (365 nm) at 195 K.

through photochemically allowed conrotatory mode. Indeed, *anti*-**3** was converted into *Z*-**2** by UV irradiation. Notably, the ring-opening reaction did not proceed thermally by heating even at 393 K in degassed toluene. On the other hand, although the reconversion of *Z*-**2** to *anti*-**3** is also expected to be a photochemically allowed process, irradiation (700 nm) of *Z*-**2** in a MTHF matrix resulted in no perceptible change in the electronic absorption spectrum. In contrast, *Z*-**2** demonstrated the thermal ring-closure reaction in conrotatory mode, which is not conforming to the Woodward–Hoffmann rule, being investigated by spectroscopic analyses.

Thermal ring-closure reaction of *E*-**2** was monitored by ^{1}H NMR spectroscopy. The signals of *E*-**2** generated in degassed dichloromethane-d_2 almost disappeared after storing in the dark for 1 h, and the peaks of *anti*-**3** were recovered (Figure 7). This result suggests that *E*-**2** underwent the kinetically unfavorable conrotatory ring-closure even at 298 K. It should be noted that *syn*-**3**, which would be a product of a kinetically favorable disrotatory process, was not found in ^{1}H NMR spectrum. Detailed kinetics of the thermal ring-closure was studied by time dependence of the electronic absorption spectrum. As shown in Figure 8a, the absorption band of *E*-**2** at 619 nm decayed with a simple first-order kinetics, and an intense absorption band attributed to *anti*-**3** at shorter wavelength region was recovered. *E*-**2** is expected to undergo the ring-closure reaction in a stepwise pathway via *Z*-**2** as an intermediate. The activation barrier of *E*–*Z* isomerization determined experimentally was substantially low; thus, the ring-closure step from *Z*-**2** to *anti*-**3** should be the rate-determining step. The activation barrier for the rate-determining step was estimated from the temperature dependence of a decay rate constant to be 15.7 ± 1.0 kcal mol^{-1} (log*A* = 7.9) by using Arrhenius plot (Figure 8b).

Computational Studies. Detailed calculations of the molecular geometries and electronic structures of *E*,*Z*-**2** and *anti*-**3** were reported by Agranat et al.,[17] which suggested the singlet biradical ground states of *E*,*Z*-**2**. Here we focus on the molecular orbitals and ground state description of *E*,*Z*-**2** and *anti*-**3** to account for their unique reactivity. The singlet biradical indices y_0 of *E*,*Z*-**2** were estimated with CASSCF(2,2)/6-31G**//UB3LYP(BS)/6-31G** and UB3LYP(BS)/6-31G** methods. A CASSCF(2,2)/6-31G**//UB3LYP(BS)/6-31G** calculation gave an admixture of 14% of the doubly excited configuration into the ground state description of *E*-**2**; thus, the y_0 of *E*-**2** was estimated to be 28%. A broken-symmetry UB3LYP/6-31G** calculation gave a similar value; the natural orbital occupancy number (NOON) of LUMO of *E*-**2** is 0.36, indicating the y_0 of 36%. The y_0 of *Z*-**2** was also determined with the same calculation methods to be 67% and 94%, respectively, which indicates that the biradical character of *Z*-**2** with a larger twisted angle is considerably larger than that of *E*-**2**.

Molecular orbitals of *Z*-**2** and *anti*-**3** reflect the electronic structures of *cis*-1,3,5-hexatriene and 1,3-cyclohexadiene, respectively (shown in Figure S5). Thus, the thermal ring-closure in conrotatory fashion should be a kinetically unfavorable pathway according to the Woodward–Hoffmann rule. To gain an energetic insight into the ring-closure process, the transition states in conrotatory (TS1) and disrotatory (TS2) modes were estimated with a UB3LYP(BS)/6-31G** method (Figure 9). The activation barrier for conrotatory ring-closure process was estimated to be 22.6 kcal mol^{-1}, which is comparable with that reported in the previous literature by Agranat et al. (28.6 kcal mol^{-1} at UB3LYP/6-31G* level)[17] and the experimental value (15.7 ± 1.0 kcal mol^{-1}). In contrast to the facility of the conrotatory process, larger activation energy (30.8 kcal mol^{-1}) is required for the disrotatory process. The overall energy diagram is displayed in Figure 10. The activation barrier for *E*–*Z* isomerization of *Z*-**2** (TS3) was calculated to be 0.8 kcal mol^{-1}, which is considerably lower than that of general alkenes but is consistent with the estimation from transient absorption measurements (4.3 ± 0.3 kcal mol^{-1}). The computational results predict that *E*,*Z*-**2** exhibit the dynamic equilibrium; thus, the ring-closure step from *Z*-**2** to *anti*-**3** should be a rate-determining step of thermal ring-closure reaction.

In addition, S_1 energies were estimated by using a spin flip TDDFT calculations at BHHLYP/6-311G* level to elucidate the mechanism of the photoinduced ring-opening reaction of *anti*-**3** to *Z*-**2** (shown in Figure 11). Spin flip TDDFT calculation is a sophisticated method to estimate the electronic structure of the excited states of singlet biradical species. Singlet biradicals are known to have a low-lying doubly excited states (HOMO,HOMO → LUMO,LUMO);[24] thus, detailed assignments of the S_1 states of *E*,*Z*-**2** are required for the mechanistic studies on the photoinduced ring-opening reaction. The computational results suggest that the HOMO,HOMO → LUMO,LUMO doubly excited states are always higher in

DOI: 10.1021/jacs.5b13033
J. Am. Chem. Soc. XXXX, XXX, XXX–XXX

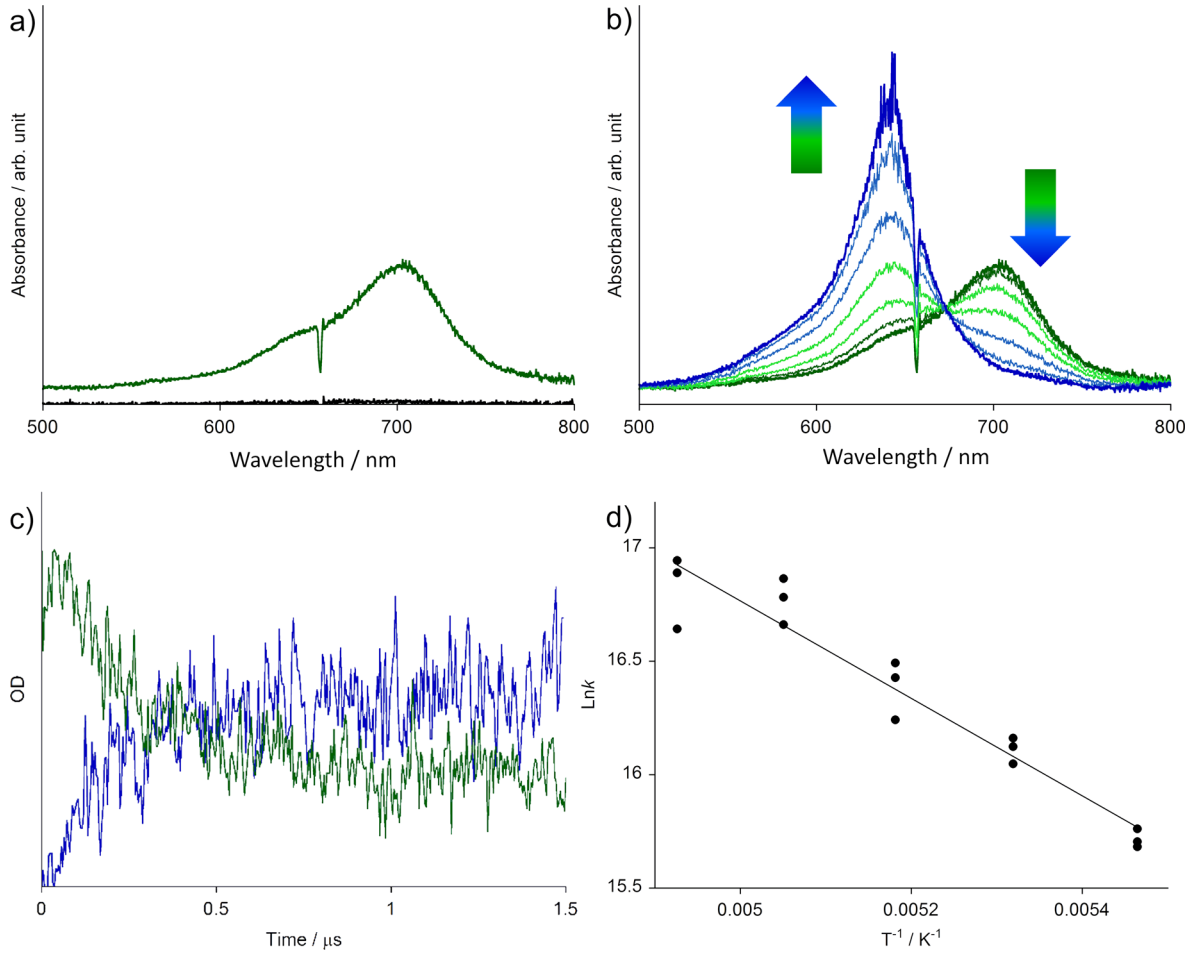

Figure 6. (a) Differential electronic absorption spectrum of *Z*-**2** generated by UV irradiation (355 nm) in a MTHF matrix (1×10^{-4} M) at 98 K. (b) Differential absorption spectra measured periodically at 120 K. (c) Transient absorption dynamics measured in MTHF (1×10^{-4} M) at 175 K. The decay rate of *Z*-**2** and the glow rate of *E*-**2** were monitored at 705 and 630 nm, respectively. (d) Arrhenius plot to determine the activation barrier for thermal isomerization from *Z*-**2** to *E*-**2**.

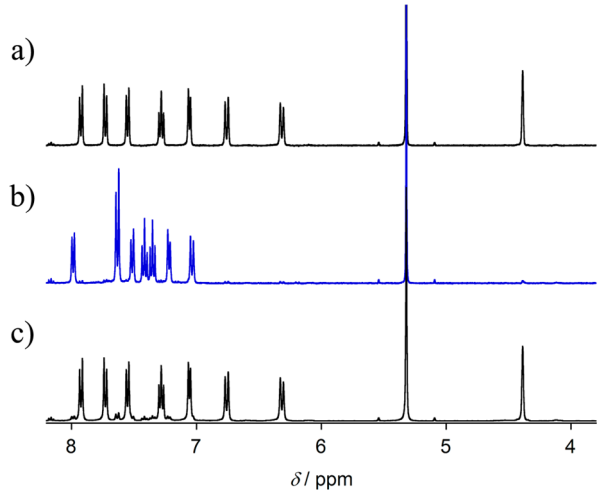

Figure 7. ^{1}H NMR spectra measured in dichloromethane-d_2 at 183 K (a) before irradiation, (b) just after irradiation UV light (365 nm), and (c) after storing in the dark for 1 h.

energy than the HOMO → LUMO singly excited state. Therefore, the S_1 state dominating the photochemical reaction is ascribed to the singly excited state, and the doubly excited state is assignable to the S_2 state. The structural relaxation of *anti*-**3** in the S_1 state results in the changes of the twisted angle between two phenalenyl moieties and the bond lengths of the central six-membered ring, leading to the formation of *Z*-**2** in exothermic process. In contrast, the conrotatory ring-closure of *Z*-**2** to *anti*-**3**, which is expected to be a photochemically allowed path according to the Woodward–Hoffmann rule, is energetically uphill on the S_1 energy surface. Therefore, the photoinduced ring-closure reaction of *Z*-**2** was not observed at least in the experimental condition conducted at 98 K. The structural optimization in the S_1 state by the BHHLYP spin flip TDDFT calculation gives two local minima, *Z*-**2′** between *Z*-**2** and TS3 found in the UB3LYP TDDFT calculation, and *E*-**2′** between *E*-**2** and TS3, depending on the initial structures *E*-**2** or *Z*-**2**. This indicates the presence of an activation barrier between *Z*-**2′** and *E*-**2′** in the S_1 potential energy surface. Frequency analyses with spin flip TDDFT were not performed due to its computational cost. Thus, the photoinduced ring-opening reaction is considered to proceed by *anti*-**3**(S_0) → *anti*-**3**(S_1) → *Z*-**2′**(S_1) → *Z*-**2′**(S_0) → *Z*-**2**(S_0) process. This computational prediction strongly supports the experimental results of spectroscopic analyses that *Z*-**2** was generated selectively by the photoinduced ring-opening reaction of *anti*-**3**.

Decomposition of Dihydroperopyrene to Peropyrene. *anti*-**3** showed a gradual decomposition in air-saturated solution. Storing the solution of *anti*-**3** in air resulted in the

DOI: 10.1021/jacs.5b13033
J. Am. Chem. Soc. XXXX, XXX, XXX−XXX

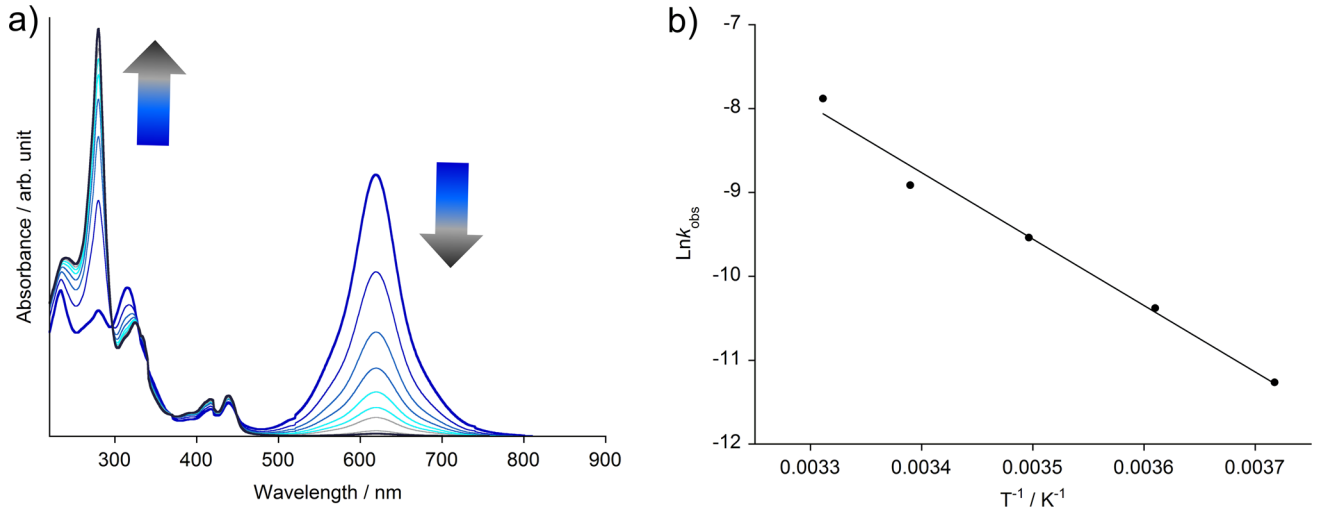

Figure 8. (a) Time dependence of the electronic absorption spectra of *E*-**2** measured in dichloromethane (1×10^{-5} M) at room temperature. (b) Arrhenius plot to determine the activation barrier for the ring-closure process.

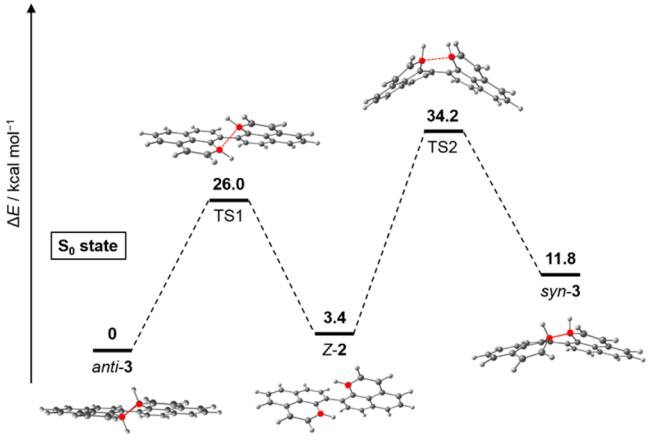

Figure 9. Energy diagram of the electrocyclic reaction in conrotatory and disrotatory processes. Transition states were identified by one imaginary frequency at the saddle point. The relative energies were estimated after ZPE correction.

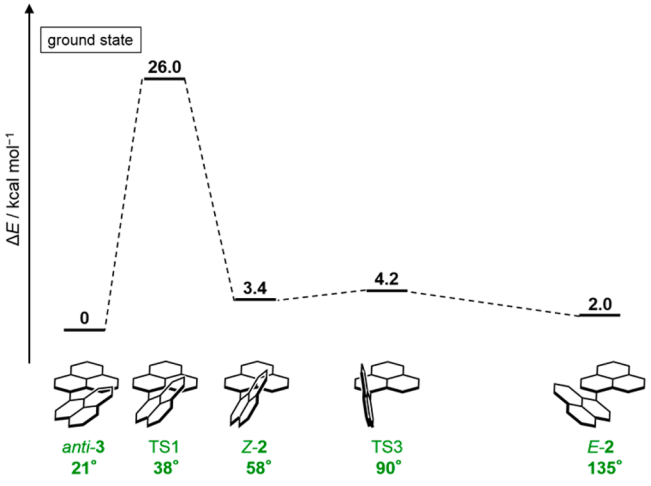

Figure 10. Energy diagram calculated with a UB3LYP(BS)/6-31G** method. Transition states were identified by one imaginary frequency at the saddle point. The relative energies were estimated after ZPE correction.

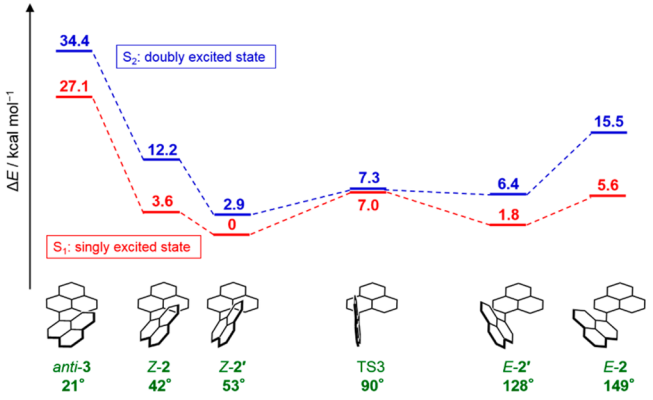

Figure 11. Energy diagram calculated with a spin flip TDDFT calculation at BHHLYP/6-311G* level. The structures of *E,Z*-**2** and *anti*-**3** were optimized by a spin flip TDDFT calculations at BHHLYP/6-311G* level. The energies of TS3 in the excited states were calculated with the geometry obtained by a UB3LYP(BS)/6-31G** method.

substantial change in ^{1}H NMR spectrum (Figure 12), and approximately 50% of *anti*-**3** decomposed after 2 weeks to give orange crystals of peropyrene **4**. The decomposed product was unambiguously assigned to **4** by X-ray crystallographic analysis. The crystal structure of **4** was almost identical to that reported previously by Bardeen et al.[25] A half-life of *anti*-**3** in air-saturated solution was estimated to be 11 days from intensity change of ^{1}H NMR signals.

Direct Observation of the Decomposed Products of the Parent Phenalenyl. Previous reports described that the generation of **1** by the dehydrogenation of phenalene is accompanied by the formation of blue or green products that show an absorption band centered at 613 nm.[16] We suspected that the colored species is *E*-**2**. To an excess amount of phenalene was added *p*-chloranil in degassed dichloromethane, and the electronic absorption spectra were recorded periodically. Actually, a characteristic absorption band centered at 620 nm was observed in the early stage of the reaction, and then, the absorption gradually decreased in intensity and disappeared within 1 h, along with increasing the band intensity of peropyrene (390, 414, and 441 nm), as shown in Figure 13.

DOI: 10.1021/jacs.5b13033
J. Am. Chem. Soc. XXXX, XXX, XXX−XXX

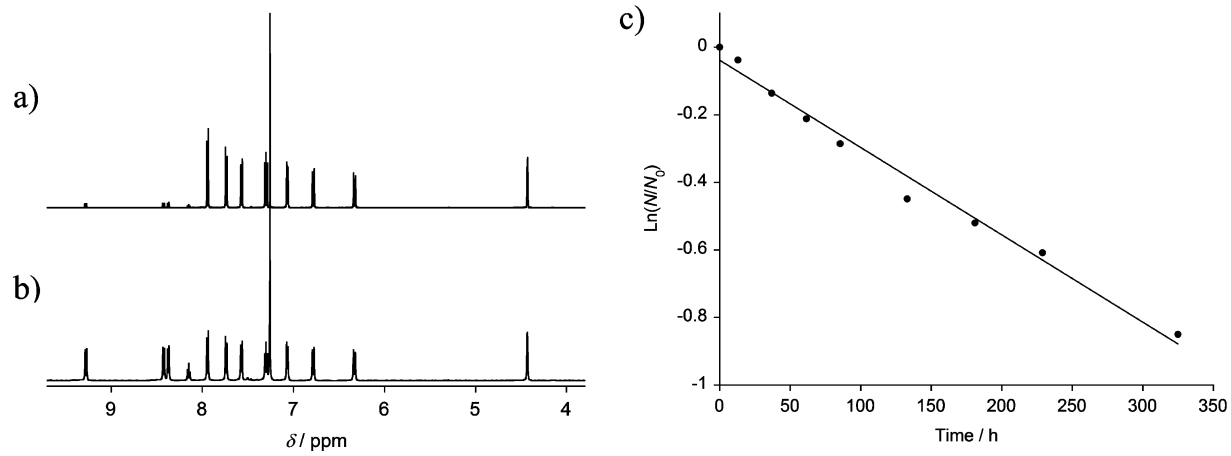

Figure 12. ^{1}H NMR spectra of *anti*-**3** recorded (a) just after preparation, and (b) after storing in air-saturated $CDCl_3$ for 2 weeks. Hexamethylbenzene was used as an internal standard to normalize the intensity of *anti*-**3** signals. (c) Determination of a half-life of *anti*-**3** at room temperature from the time dependence of a signal intensity corresponding to benzyl protons of *anti*-**3**.

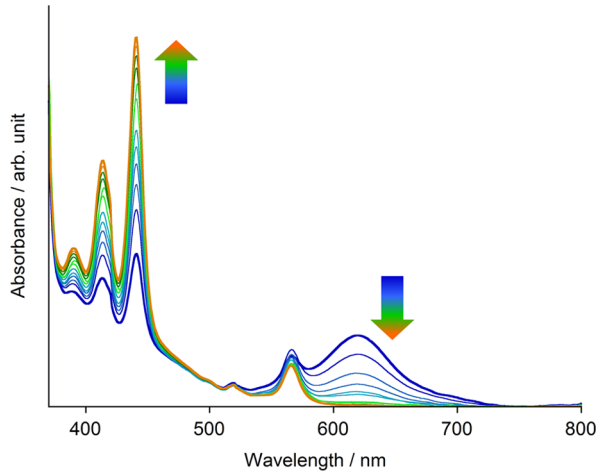

Figure 13. Electronic absorption spectra of phenalenyl **1** in dichloromethane (2×10^{-5} M). The spectra were measured periodically after preparation of **1** (every 10 min for 1 h, then 1.5, 2, 3, 4, 5, and 6.5 h).

The feature of the absorption band at 620 nm is identical to that of *E*-**2**, suggesting strongly that *E*-**2** exists as an intermediate on the decomposition pathway of **1**. Notably, a weak band observed at 565 nm, which would arise from **1**, remained unchanged for a couple of days after disappearance of *E*-**2**, suggesting the persistency of **1** in the condition without any oxidants.

DISCUSSION

E,Z-**2** exhibited the unusual reactions: conrotatory ring-closure to *anti*-**3**, and rapid *E*−*Z* isomerization. The thermal ring-closure in conrotatory process is kinetically unfavorable process for *cis*-1,3,5-hexatriene analogues with respect to the disrotatory process according to the Woodward−Hoffmann predictions, whereas *Z*-**2** demonstrated a facile ring-closure in conrotatory fashion to give *anti*-**3**. Moreover, *E,Z*-**2** underwent a rapid *E*−*Z* isomerization. The activation energy determined experimentally is extremely small (4.3 ± 0.3 kcal mol^{-1}) compared to that for isomerization of general alkenes. These unique reactivities of *E,Z*-**2** are ascribed to their singlet biradical nature.

1,3-Cyclohexadiene and *cis*-1,3,5-hexatriene analogues that show the unusual electrocyclization were shown in Scheme 3.

Scheme 3. (a and b) Thermal Electrocyclization in Conrotatory Process between 1,3-Cyclohexadiene and *cis*-1,3,5-Hexatriene Analogues; (c) Thermal Reactions Demonstrated by Pleiadene Derivatives

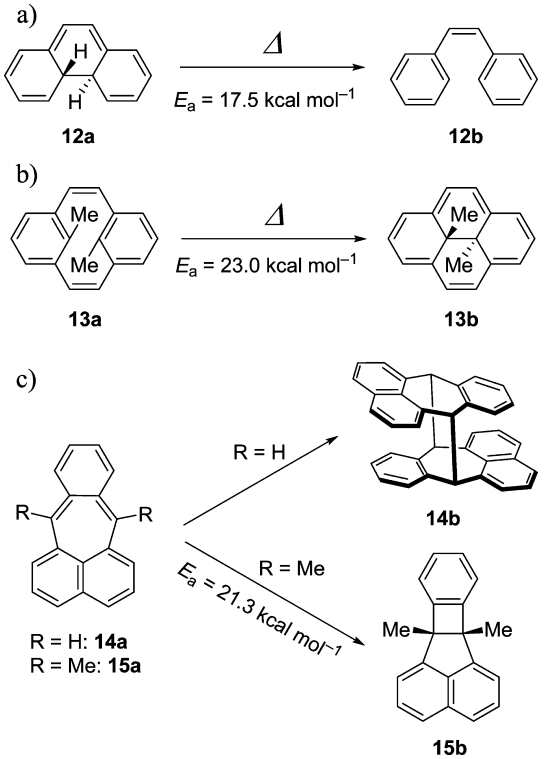

4a,4b-Dihydrophenanthrene (**12a**), which is analogous to 1,3-cyclohexadiene, is well-known to demonstrate a facile ring-opening in conrotatory process to afford *cis*-stilbene (**12b**).[26] Loss of aromatic stabilization energy destabilizes **12a** with respect to **12b**, resulting in the decrease of a relative activation barrier to induce the thermal ring-opening in conrotatory fashion. On the other hand, **13a** undergoes a thermal ring-closure in conrotatory mode to give corresponding 1,3-cycrohexadiene analogue (**13b**).[27,28] In this case, the structural

DOI: 10.1021/jacs.5b13033
J. Am. Chem. Soc. XXXX, XXX, XXX−XXX

strain of **13a** leads to the conrotatory ring-closure not conforming to the Woodward–Hoffmann prediction.

The orbital symmetry forbidden reaction of the singlet biradical species was reported by Michl et al.[29,30] Pleiadene is a singlet biradical compound having the *o*-quionodimethane scaffold. The parent pleiadene (**14a**) showed a facile dimerization to form **14b** owing to its singlet biradical ground state,[29,31] whereas a dimethyl derivative (**15a**) underwent the intramolecular ring-closure in disrotatory process to give a corresponding cyclobutene derivative (**15b**).[30] The thermal interconversion between 1,3-butadiene and cyclobutene in disrotatory mode is expected to be a kinetically unfavorable process by the Woodward–Hoffmann rule, whereas the activation energy for the ring-closure reaction is considerably small (21.3 kcal mol^{-1}). The facile ring-closure was accounted for by the destabilized ground state of pleiadene due to its singlet biradical character. A small HOMO–LUMO gap of the singlet biradical species leads to an admixture of the doubly excited configuration into the ground state description, resulting in the decrease of covalent bonding interactions and destabilization of the ground state.

The unusual ring-closure reaction of *Z*-**2** can be rationalized by the destabilized ground state of *Z*-**2**. Indeed, the contribution of the doubly excited configuration to the ground state description was corroborated by the CASSCF(2,2)/6-31G**//UB3LYP(BS)/6-31G** calculation (see above). The admixture of the doubly excited configuration results in the destabilization of the ground state of *Z*-**2**, decreasing the relative activation barrier for the conrotatory ring-closure reaction. In contrast, the activation energy of the disrotatory process is considerably larger. With a focus on the computational result, the transition structure of disrotatory ring-closure process (TS2 in Figure 9) is highly contorted, leading to the large activation energy. Therefore, the ring-closure in conrotatory process is the kinetically and thermodynamically favored process, which is fully consistent with the experimental finding that thermal ring-closure of *Z*-**2** solely gave *anti*-**3**.

The facile *E*–*Z* isomerization is also ascribed to the biradical ground states of *E*,*Z*-**2**. The destabilized ground states of *E*,*Z*-**2** lead to the decrease of an activation barrier for the isomerization. In addition, the transition state for the isomerization (TS3 in Figure 10) is stabilized in comparison with that for general alkenes. The isomerization of alkene is considered to proceed through a biradical transition structure as illustrated in Scheme 4. In the case of **2**, the biradical transition state can be stabilized thermodynamically by the delocalization of unpaired electrons over phenalenyl moieties. Thus, the combination of destabilization of the ground state of *E*,*Z*-**2** and stabilization of TS3 leads to the facility of *E*–*Z* isomerization.

CONCLUSIONS

In summary, first isolation of *E*,*Z*-biphenalenylidene (*E*,*Z*-**2**) in solution state was accomplished by means of the photoinduced electrocyclic ring-opening reaction of *anti*-dihydroperopyrene (*anti*-**3**). The structural characterizations of *E*,*Z*-**2** and *anti*-**3** were performed by spectroscopic analyses (^{1}H NMR and electronic absorption measurements) as well as computational studies. *Z*-**2**, which was trapped in a rigid matrix of a solvent, demonstrated the rapid *E*–*Z* isomerization to *E*-**2**, and the kinetic investigation indicated that the activation barrier of 4.3 ± 0.3 kcal mol^{-1} is extraordinarily smaller than that of general alkenes. Furthermore, *Z*-**2** showed the unusual ring-closure reaction in conrotatory process to afford *anti*-**3**, which is against the Woodward–Hoffmann prediction. The activation barrier was also determined by spectroscopic techniques to be 15.7 ± 1.0 kcal mol^{-1}. These unique reactions can be rationalized by the singlet biradical nature of *E*,*Z*-**2**. Admixture of the doubly excited configuration into the ground state description resulted in the decrease of the intramolecular covalent bonding interaction and destabilized the ground states of *E*,*Z*-**2**. In addition, the biradical transition state of *E*–*Z* isomerization (TS3 in Figure 10) was stabilized by the delocalization of unpaired electrons over phenalenyl moieties, facilitating the unusual *E*–*Z* isomerization.

Scheme 4. *E*–*Z* Isomerization of (a) Alkenes and (b) *E*,*Z*-2 through Biradical Transition Structures

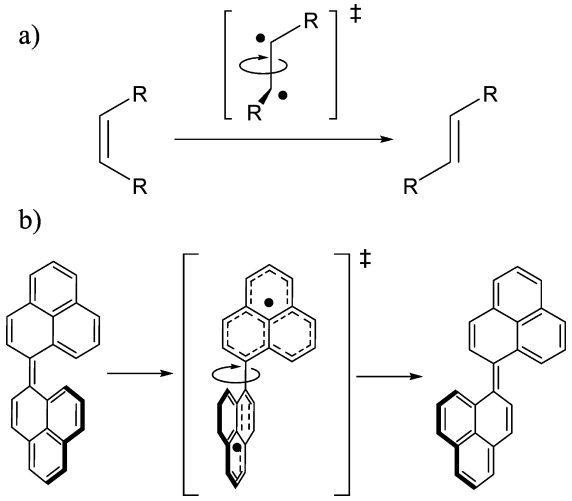

Deeper understanding of the electronic structure and reactivities of *E*,*Z*-**2** and *anti*-**3** enabled us to confirm the decomposition mechanism of the parent phenalenyl (**1**). The presence of *E*-**2** in the decomposition pathway was unambiguously corroborated; thus, the colored product reported in previous literatures[14−16] was not the desired product **1** but the decomposed product *E*-**2**. The decomposition of **1** in the presence of oxidants proceeds as the following mechanisms: (1) **1** exists as an equilibrium mixture with $\mathbf{1}_2$ *σ*-dimer, (2) dehydrogenation of $\mathbf{1}_2$ *σ*-dimer gives *E*,*Z*-**2**, (3) thermal *E*–*Z* isomerization and conrotatory ring-closure lead to *anti*-**3**, and then (4) dehydrogenation of *anti*-**3** forms peropyrene **4** as a final product.

EXPERIMENTAL SECTION

General. All experiments with moisture- or air-sensitive compounds were performed in anhydrous solvents under nitrogen atmosphere in well-dried glassware. Dried solvents were prepared by distillation under nitrogen. Toluene and DMF were dried and distilled over calcium hydride. 2-Methyltetrahydrofuran (MTHF) was dried and distilled over sodium. Anhydrous dichloromethane was purchased from Kanto Chemical Co., Inc. and used without further purification. Column chromatography was performed with silica gel [Silica gel 60N (Kanto Chemical Co., Inc.)]. Melting points were taken on a Yanako MP 500D apparatus. ^{1}H NMR and ^{13}C NMR spectra were obtained on JEOL ECS400 and ECA500 spectrometers. The chemical shifts were recorded by using tetramethylsilane (0.00 ppm) as an internal standard for ^{1}H NMR and $CHCl_3$ (77.00 ppm) for ^{13}C NMR spectra. Positive EI mass spectra were taken by using Shimadzu QP-5050. High resolution mass spectra were analyzed by using Applied Biosystems Japan Ltd. Analyst QS 2.0. Data collection for X-ray crystal analysis was performed on Rigaku/Varimax diffractometer (Mo-K*α*, *λ* =

DOI: 10.1021/jacs.5b13033
J. Am. Chem. Soc. XXXX, XXX, XXX−XXX

0.71069 Å). The structure was solved with direct methods and refined with full-matrix least-squares (teXsan). Infrared spectra were recorded on a JASCO FT/IR-660 M spectrometer. Steady-state UV−vis absorption spectra were measured in anhydrous dichloromethane and MTHF with a JASCO V-570 spectrometer. The nanosecond time-resolved difference absorption spectra were obtained using the third harmonic (THG) of a Nd^{3+}:YAG laser (Continuum Mini-lite II, λ_{ex} = 355 nm, 4−6 ns pulse width, 7 mJ) for the excitation. The monitoring system comprised a 150-W Xe lamp as the light source, a UNISOKU-MD200 monochromator, and a photomultiplier.

Computational Details. All geometry optimizations and transition state calculations were performed with the Gaussian 09 program. The optimized structures of *E,Z*-**2** and *syn,anti*-**3** have no imaginary frequency, and the transition structures have one imaginary frequency at the saddle points. The single point calculations with UB3LYP/6-31G**, RHF/6-31G**, and CASSCF(2,2)/6-31G** methods were conducted with the optimized geometries calculated at UB3LYP(BS)/6-31G** level of theory by using the Gaussian 03 program. TD-UB3LYP(BS)/6-31G** and GIAO-(U)B3LYP/6-31G** calculations were also performed with the optimized geometries obtained by a UB3LYP(BS)/6-31G** method. Spin-flip TDDFT calculation was performed with the GAMESS 2014 program package, employing the BHHLYP exchange-correlation functional and the 6-311G* basis set because the SF-DFT benchmark calculations show a better performance with hybrid functionals including a larger fraction of HF exchange, e.g., 50% HF plus 50% Becke exchange, than that with the conventional B3LYP functional.[32,33]

4,4′-Dibromo-1,1′-binaphthalene (6). 1,1′-Binaphthalene **5** (0.79 g, 3.1 mmol) was dissolved in chloroform (30 mL) and the solution was cooled to 0 °C with an ice-bath. To the solution was added bromine (2.6 g, 16 mmol) over 20 min. After the mixture stirred for 2.5 h, aqueous sodium sulfite was added for quenching. The organic layer was separated and washed with brine, dried over anhydrous sodium sulfate. After filtration, the filtrate was evaporated and the residue was recrystallized from chloroform to give **6** as a white crystal (0.82 g, 64%). Mp 217−219 °C; R_f = 0.48 (hexane); ^{1}H NMR (400 MHz, $CDCl_3$) δ 8.36 (d, J = 8.8 Hz, 2H), 7.90 (d, J = 7.6 Hz, 2H), 7.62−7.58 (m, 2H), 7.35−7.31 (m, 6H); ^{13}C NMR (126 MHz, $CDCl_3$) δ 137.63, 133.83, 131.93, 129.44, 128.11, 127.45, 127.39, 126.98, 126.92, 123.00.

Dimethyl 3,3′-([1,1′-Binaphthalene]-4,4′-diyl)(2*E*,2′*E*)-diacrylate (7). A flask was charged with 4,4′-dibromo-1,1′-binaphthalene **6** (0.50 g, 1.2 mmol), palladium(II) acetate (54 mg, 0.24 mmol), triphenylphosphine (0.13 g, 0.49 mmol), potassium carbonate (0.67 g, 4.9 mmol), and tetrabutylammonium bromide (2.0 g, 6.2 mmol) under nitrogen atmosphere. Methyl acrylate (0.33 mL, 3.6 mmol) in DMF (25 mL) was added, and the solution was heated at 80 °C for 11 h. After the solution cooled to room temperature, the precipitates were filtered out, and the filtrate was poured into water. The reaction mixture was extracted with dichloromethane, and the organic layer was washed with water and brine, dried over anhydrous sodium sulfate. After filtration, the filtrate was evaporated and the residue was purified by column chromatography on silica gel (dichloromethane/hexane 75%) to give **7** as a white solid (0.48 g, 93%). Mp 203−204 °C; R_f = 0.14 (dichloromethane/hexane 50%); ^{1}H NMR (400 MHz, $CDCl_3$) δ 8.64 (d, J = 15.6 Hz, 2H), 8.30 (d, J = 8.4 Hz, 2H), 7.87 (d, J = 7.6 Hz, 2H), 7.58 (td, J = 6.8 Hz, 1.6 Hz, 2H), 7.50 (d, J = 7.6 Hz, 2H), 7.43 (dd, J = 8.8 Hz, 1.6 Hz, 2H), 7.35 (td, J = 6.8 Hz, 1.6 Hz, 2H), 6.63 (d, J = 15.6 Hz, 2H), 3.89 (s, 6H); ^{13}C NMR (126 MHz, $CDCl_3$) δ 167.29, 141.80, 140.56, 132.86, 131.91, 131.46, 127.44, 127.21, 126.89, 126.46, 124.48, 123.65, 120.75, 51.85; IR (KBr) ν = 3044 (w), 2991 (w), 2947 (m), 2844 (w), 2367 (w), 1714 (s), 1630 (s), 1576 (m), 1437 (s), 1381 (m), 1307 (s), 1249 (m), 1230 (m), 1194 (s), 1174 (s), 1114 (m), 977 (s), 844 (s), 768 (s) cm^{-1}; EI-MS m/z 422 (M^+); Anal. Calcd for $C_{28}H_{22}O_4$: C, 79.60; H, 5.25. Found: C, 79.33; H, 5.21.

Dimethyl 3,3′-([1,1′-Binaphthalene]-4,4′-diyl)dipropionate (8). Dimethyl 3,3′-([1,1′-binaphthalene]-4,4′-diyl)(2*E*,2′*E*)-diacrylate **7** (0.45 g, 1.1 mmol) was dissolved in dichloromethane (10 mL) and ethyl acetate (90 mL); then 10% Pd−C (50 mg, 10 wt %) was added. The reaction mixture was stirred for 3 h under hydrogen atmosphere. After removal of Pd−C by filtration, filtrate was evaporated. The residue was purified by column chromatography on silica gel (dichloromethane/hexane 70%) to give **8** as a colorless oil (0.40 g, 88%). R_f = 0.14 (dichloromethane/hexane 50%); ^{1}H NMR (400 MHz, $CDCl_3$) δ 8.12 (d, J = 8.8 Hz, 2H), 7.52 (td, J = 6.8 Hz, 1.5 Hz, 2H), 7.45 (d, J = 6.8 Hz, 2H), 7.41 (dd, J = 8.4 Hz, 0.8 Hz, 2H), 7.39 (d, J = 6.8 Hz, 2H), 7.28 (td, J = 6.4 Hz, 0.8 Hz, 2H), 3.75 (s, 6H), 3.55−3.51 (m, 4H), 2.90−2.86 (m, 4H); ^{13}C NMR (126 MHz, $CDCl_3$) δ 173.50, 137.55, 136.23, 133.29, 131.57, 127.56 (broad, 2C), 125.95, 125.62, 125.42, 123.51, 51.74, 34.98, 28.23; IR (KBr) ν = 3068 (w), 3010 (w), 2950 (m), 2844 (w), 1737 (s), 1590 (w), 1512 (w), 1436 (s), 1364 (m), 1295 (m), 1256 (s), 1198 (s), 1170 (s), 1029 (w), 984 (w), 842 (m), 765 (s) cm^{-1}; HRMS (ESI, positive): m/z Calcd for $C_{28}H_{26}O_4Na$: 449.1723 $[M + Na]^+$. Found: 449.1729.

3,3′-([1,1′-Binaphthalene]-4,4′-diyl)dipropionic Acid (9). To a solution of dimethyl 3,3′-([1,1′-binaphthalene]-4,4′-diyl)-dipropionate **8** (0.40 g, 0.94 mmol) in ethanol (30 mL) was added 10% aqueous sodium hydroxide (15 mL), and the solution was heated at 90 °C for 14 h. After the solution cooled to room temperature, the reaction mixture was poured into 6 M hydrochloric acid and extracted with ether. The organic layer was separated and washed with brine, dried over anhydrous sodium sulfate. After filtration, the filtrate was evaporated, and then the residue was collected and washed with ether to give **9** as a white powder (0.35 g, 94%). Mp 256−257 °C; R_f = 0.07 (ethyl acetate/hexane 50%); ^{1}H NMR (400 MHz, Acetone-d_6) δ 8.25 (d, J = 8.4 Hz, 2H), 7.59−7.55 (m, 4H), 7.42 (d, J = 7.2 Hz, 2H), 7.33−7.32 (m, 4H), 3.53 (t, J = 8.0 Hz, 4H), 2.87 (t, J = 8.0 Hz, overlapped with a broad proton signal of carboxyl group); ^{13}C NMR (126 MHz, DMSO-d_6) δ 173.87, 136.71, 136.57, 132.57, 131.27, 127.31, 126.64, 126.06, 125.81, 125.31, 123.87, 34.53, 27.49; IR (KBr) ν = 3040 (m), 2936 (m), 2688 (m), 2611 (m), 1705 (s), 1592 (w), 1513 (w), 1424 (m), 1384 (m), 1303 (m), 1211 (m), 936 (w), 836 (m), 765 (m) cm^{-1}; HRMS (ESI, positive): m/z Calcd for $C_{26}H_{22}O_4Na$: 421.1410 $[M + Na]^+$. Found: 421.1415.

4,4′,5,5′-Tetrahydro-6*H*,6′*H*-[1,1′-biphenalene]-6,6′-dione (10). 3,3′-([1,1′-Binaphthalene]-4,4′-diyl)dipropionic acid **9** (0.34 g, 0.85 mmol) was dissolved in oxalyl chloride (20 mL) and heated at 60 °C for 14 h. After removal of excess oxalyl chloride under reduced pressure, the residue was dissolved in dichloromethane (30 mL) and cooled to −78 °C under nitrogen atmosphere. To the solution was added aluminum chloride (0.46 mg, 3.4 mmol). The reaction mixture was stirred at −78 °C for 2 h, then warmed gradually to −30 °C. The reaction was quenched with 1 M hydrochloric acid and extracted with dichloromethane. The organic layer was separated and washed with aqueous sodium carbonate, dried over anhydrous sodium sulfate. After filtration, the filtrate was evaporated and the residue was purified by column chromatography on silica gel (dichloromethane/hexane 70%) to give **10** as a pale yellow powder (0.27 g, 88%). Mp 216 °C (decomposition); R_f = 0.15 (dichloromethane/hexane 70%); ^{1}H NMR (400 MHz, $CDCl_3$) δ 8.22 (d, J = 7.2 Hz, 2H), 7.64 (d, J = 8.4 Hz, 2H), 7.59 (d, J = 6.8 Hz, 2H), 7.50 (d, J = 7.2 Hz, 2H), 7.43 (t, J = 7.6 Hz, 2H), 3.55 (t, J = 7.2 Hz, 4H), 3.08 (t, J = 7.2 Hz, 4H); ^{13}C NMR (126 MHz, $CDCl_3$) δ 198.47, 136.39, 133.31, 132.78, 132.57, 131.70, 129.98, 128.28, 125.87, 125.25, 125.17, 38.44, 28.62; IR (KBr) ν = 3056 (w), 3018 (w), 2979 (w), 2945 (w), 2924 (w), 1691 (s), 1599 (m), 1504 (m), 1457 (m), 1434 (m), 1407 (m), 1355 (w), 1317 (m), 1276 (s), 1234 (m), 1214 (m), 1018 (m), 849 (m), 822 (s), 777 (s), 725 (s) cm^{-1}; HRMS (ESI, positive): m/z Calcd for $C_{26}H_{18}O_2Na$, 385.1199 $[M + Na]^+$. Found: 385.1205.

4*H*,4′*H*-1,1′-Biphenalene (11). To a suspension of 4,4′,5,5′-tetrahydro-6*H*,6′*H*-[1,1′-biphenalene]-6,6′-dione **10** (0.34 g, 0.94 mmol) in DCM (30 mL) and ethanol (20 mL) was added sodium borohydride (0.14 g, 3.8 mmol) under nitrogen atmosphere. After it stirred for 1 h at room temperature, the reaction was quenched with aqueous ammonium chloride. The organic layer was separated and washed with brine, dried over anhydrous sodium sulfate. After filtration, the filtrate was evaporated and the residue was purified by column chromatography on hydrous (6%) silica gel (ethyl acetate/dichloromethane 10%) to give 5,5′,6,6′-tetrahydro-4*H*,4′*H*-[1,1′-biphenalene]-6,6′-diol as a diastereomer mixture (0.28 g, 81%).

DOI: 10.1021/jacs.5b13033
J. Am. Chem. Soc. XXXX, XXX, XXX−XXX

The diastereomer mixture of the diol derivative (41 mg, 0.11 mmol) was dissolved in toluene (10 mL) under nitrogen atmosphere. To the solution was added a catalytic amount of *p*-toluenesulfonic acid monohydrate, and the solution was heated at 120 °C for 5 min. The reaction mixture was cooled at 0 °C and then the solution diluted with hexane (21 mL) was filtered rapidly on hydrous (6%) silica gel to give **11** as a pale green solid (34 mg, 92%). R_f = 0.18 (hexane); ^{1}H NMR (400 MHz, $CDCl_3$) δ 7.36−7.32 (m, 4H), 7.10−7.09 (m, 4H), 6.97 (d, J = 4 Hz, 2H), 6.64 (d, J = 10 Hz, 2H), 6.10 (m, 2H), 4.16 (s, 4H); ^{13}C NMR (126 MHz, $CDCl_3$) δ 135.85, 133.85, 132.76, 132.07, 129.41, 127.92, 127.84, 127.61, 126.24, 125.48, 124.61, 122.22, 32.28; IR (KBr) ν = 3028 (m), 2919 (s), 2853 (w), 2794 (w), 1587 (m), 1506 (w), 1415 (m), 1394 (w), 1352 (w), 1219 (w), 1054 (w), 949 (w), 837 (m), 824 (s), 764 (s), 734 (m) cm^{-1}; HRMS (ESI, positive): m/z Calcd for $C_{26}H_{17}$, 329.1325 $[M-H]^+$. Found: 329.1331.

***anti*-Dihydroperopyrene (*anti*-3).** To a solution of 4*H*,4′*H*-1,1′-biphenalene **11** (34 mg, 0.10 mmol) in toluene (10 mL) was added *p*-chloranil (27 mg, 0.11 mmol) under nitrogen atmosphere. After it stirred for 3 h, the reaction mixture was filtered rapidly on hydrous (6%) silica gel to give *anti*-**3** as a crude product. The product was reprecipitated from dichloromethane/hexane, and then the precipitate containing impurity was filtered out. The filtrate was evaporated, and the residual pale green powder was washed with hexane and collected. *anti*-**3** was obtained as a greenish yellow powder (8.0 mg, 24%). ^{1}H NMR (400 MHz, dichloromethane-d_2) δ 7.97 (d, J = 6.8 Hz, 2H), 7.76 (d, J = 6.8 Hz, 2H), 7.59 (d, J = 6.8 Hz, 2H), 7.32 (dd, J = 6.4 Hz, 5.6 Hz, 2H), 7.09 (d, J = 5.6 Hz, 2H), 6.81 (d, J = 8.0 Hz, 2H), 6.37 (d, J = 8.0 Hz, 2H), 4.42 (s, 2H); HRMS (ESI, positive): m/z Calcd for $C_{26}H_{16}$, 328.1247 $[M]^+$. Found: 328.1257.

■ ASSOCIATED CONTENT

Supporting Information

The Supporting Information is available free of charge on the ACS Publications website at DOI: 10.1021/jacs.5b13033.

Characterization data (^{1}H−^{1}H COSY, NOESY and of ROESY spectra) of *E*-**2** and *anti*-**3**, details of the time dependent electronic absorption spectra of *E*-**2** at each temperature, calculated molecular orbitals and spin density maps of *E*-**2** and *anti*-**3**, and Gaussian input data (PDF)

X-ray crystallographic data of *anti*-**3** (CIF)

■ AUTHOR INFORMATION

Corresponding Authors

*mnaka@cheng.es.osaka-u.ac.jp

*mabe@hiroshima-u.ac.jp

*kubo@chem.sci.osaka-u.ac.jp

Notes

The authors declare no competing financial interest.

■ ACKNOWLEDGMENTS

This article is dedicated to Professor Ichiro Murata on the occasion of his 88th birthday (Beijyu). K.U. and S.I. acknowledge support from the JSPS Fellowship for Young Scientists (No. 2615260 and No. 2604505, respectively). M.N. thanks a Grant-in-Aid for Scientific Research (A) (No. 25248007) from JSPS, a Grant-in-Aid for Scientific Research on Innovative Areas "Stimuli-Responsive Chemical Species" (A24109002a), "pi-System Figuration" (15H00999), "Photosynergetics" (A26107004a), MEXT, the Strategic Programs for Innovative Research (SPIRE), MEXT, and the Computational Materials Science Initiative (CMSI), Japan. Theoretical calculations are partly performed using Research Center for Computational Science, Okazaki, Japan. M.A. thanks a Grant-in-Aid for Science Research on Innovative Areas "Stimuli-responsive Chemical Species" (No. 24109008) from MEXT, Japan. T.K. thanks JSPS for KAKENHI Grant No. 26288016 and MEXT for a Grant-in-Aid for Scientific Research on Innovative Areas "Photosynergetics" (15H01086).

■ REFERENCES

(1) In phenalenyl derivatives the positions 1, 3, 4, 6, 7, and 9 are referred to as α and 2, 5, and 8 as β.

(2) Haddon, R. C. *Nature* **1975**, *256*, 394.

(3) Chi, X.; Itkis, M. E.; Patrick, B. O.; Barclay, T. M.; Reed, R. W.; Oakley, R. T.; Cordes, A. W.; Haddon, R. C. *J. Am. Chem. Soc.* **1999**, *121*, 10395.

(4) Pal, S. K.; Itkis, M. E.; Tham, F. S.; Reed, R. W.; Oakley, R. T.; Haddon, R. C. *Science* **2005**, *309*, 281.

(5) Small, D.; Rosokha, S. V.; Kochi, J. K.; Head-Gordon, M. *J. Phys. Chem. A* **2005**, *109*, 11261.

(6) Zaitsev, V.; Rosokha, S. V.; Head-Gordon, M.; Kochi, J. K. *J. Org. Chem.* **2006**, *71*, 520.

(7) Uchida, K.; Hirao, Y.; Kurata, H.; Kubo, T.; Hatano, S.; Inoue, K. *Chem. - Asian J.* **2014**, *9*, 1823.

(8) Mou, Z.; Uchida, K.; Kubo, T.; Kertesz, M. *J. Am. Chem. Soc.* **2014**, *136*, 18009.

(9) Goto, K.; Kubo, T.; Yamamoto, K.; Nakasuji, K.; Sato, K.; Shiomi, D.; Takui, T.; Kubota, M.; Kobayashi, T.; Yakusi, K.; Ouyang, J. *J. Am. Chem. Soc.* **1999**, *121*, 1619.

(10) Suzuki, S.; Morita, Y.; Fukui, K.; Sato, K.; Shiomi, D.; Takui, T.; Nakasuji, K. *J. Am. Chem. Soc.* **2006**, *128*, 2530.

(11) Fukui, K.; Sato, K.; Shiomi, D.; Takui, T.; Itoh, K.; Gotoh, K.; Kubo, T.; Yamamoto, K.; Nakasuji, K.; Naito, A. *Synth. Met.* **1999**, *103*, 2257.

(12) Koutentis, P. A.; Chen, Y.; Cao, Y.; Best, T. P.; Itkis, M. E.; Beer, L.; Oakley, R. T.; Cordes, A. W.; Brock, C. P.; Haddon, R. C. *J. Am. Chem. Soc.* **2001**, *123*, 3864.

(13) Beer, L.; Mandal, S. K.; Reed, R. W.; Oakley, R. T.; Tham, F. S.; Donnadieu, B.; Haddon, R. C. *Cryst. Growth Des.* **2007**, *7*, 802.

(14) Boekelheide, V.; Larrabee, C. E. *J. Am. Chem. Soc.* **1950**, *72*, 1245.

(15) Reid, D. H. *Tetrahedron* **1958**, *3*, 339.

(16) Reid, D. H. *Q. Rev., Chem. Soc.* **1965**, *19*, 274.

(17) Pogodin, S.; Agranat, I. *J. Am. Chem. Soc.* **2003**, *125*, 12829.

(18) Ohashi, K.; Kubo, T.; Masui, T.; Yamamoto, K.; Nakasuji, K.; Takui, T.; Kai, Y.; Murata, I. *J. Am. Chem. Soc.* **1998**, *120*, 2018.

(19) Kubo, T.; Shimizu, A.; Sakamoto, M.; Uruichi, M.; Yakushi, K.; Nakano, M.; Shiomi, D.; Sato, K.; Takui, T.; Morita, Y.; Nakasuji, K. *Angew. Chem., Int. Ed.* **2005**, *44*, 6564.

(20) Konishi, A.; Hirao, Y.; Nakano, M.; Shimizu, A.; Botek, E.; Champagne, B.; Shiomi, D.; Sato, K.; Takui, T.; Matsumoto, K.; Kurata, H.; Kubo, T. *J. Am. Chem. Soc.* **2010**, *132*, 11021.

(21) Li, Y.; Heng, W.-K.; Lee, B. S.; Aratani, N.; Zafra, J. L.; Bao, N.; Lee, R.; Sung, Y. M.; Sun, Z.; Huang, K.-W.; Webster, R. D.; López Navarrete, J. T.; Kim, D.; Osuka, A.; Casado, J.; Ding, J.; Wu, J. *J. Am. Chem. Soc.* **2012**, *134*, 14913.

(22) Shimizu, A.; Kishi, R.; Nakano, M.; Shiomi, D.; Sato, K.; Takui, T.; Hisaki, I.; Miyata, M.; Tobe, Y. *Angew. Chem., Int. Ed.* **2013**, *52*, 6076.

(23) Tomioka, H. *Advances in Strained and Interesting Organic Molecules*; Halton, B., Ed.; JAI Press: Greenwich, CT, 2000; Vol. *8*, p 83.

(24) Di Motta, S.; Negri, F.; Fazzi, D.; Castiglioni, C.; Canesi, E. V. *J. Phys. Chem. Lett.* **2010**, *1*, 3334.

(25) Nichols, V. M.; Rodriguez, M. T.; Piland, G. B.; Tham, F.; Nesterov, V. N.; Youngblood, W. J.; Bardeen, C. J. *J. Phys. Chem. C* **2013**, *117*, 16802.

(26) Muszkat, K. A.; Fischer, E. *J. Chem. Soc. B* **1967**, 662.

(27) Boekelheide, V.; Phillips, J. B. *J. Am. Chem. Soc.* **1967**, *89*, 1695.

(28) Blattmann, H.-R.; Schmidt, W. *Tetrahedron* **1970**, *26*, 5885.

(29) Kolc, J.; Michl, J. *J. Am. Chem. Soc.* **1970**, *92*, 4147.

(30) Steiner, R. P.; Michl, J. *J. Am. Chem. Soc.* **1978**, *100*, 6413.

DOI: 10.1021/jacs.5b13033
J. Am. Chem. Soc. XXXX, XXX, XXX−XXX

(31) Cava, M. P.; Schlessinger, R. H. *Tetrahedron* **1965**, *21*, 3073.
(32) Shao, Y.; Head-Gordon, M.; Krylov, A. I. *J. Chem. Phys.* **2003**, *118*, 4807.
(33) Minami, T.; Ito, S.; Nakano, M. *J. Phys. Chem. A* **2013**, *117*, 2000.

DOI: 10.1021/jacs.5b13033
J. Am. Chem. Soc. XXXX, XXX, XXX−XXX